

High-Permeability Magnetic Polymer Additives for Lightweight Electromagnetic Shielding

by Kristen S Williams and B Christopher Rinderspacher

ARL-TR-7372

August 2015

NOTICES

Disclaimers

The findings in this report are not to be construed as an official Department of the Army position unless so designated by other authorized documents.

Citation of manufacturer's or trade names does not constitute an official endorsement or approval of the use thereof.

Destroy this report when it is no longer needed. Do not return it to the originator.

Army Research Laboratory

Aberdeen Proving Ground, MD 21005-5066

ARL-TR-7372**August 2015**

High-Permeability Magnetic Polymer Additives for Lightweight Electromagnetic Shielding

Kristen S Williams and B Christopher Rinderspacher
Weapons and Materials Research Directorate, ARL

REPORT DOCUMENTATION PAGE				Form Approved OMB No. 0704-0188	
Public reporting burden for this collection of information is estimated to average 1 hour per response, including the time for reviewing instructions, searching existing data sources, gathering and maintaining the data needed, and completing and reviewing the collection information. Send comments regarding this burden estimate or any other aspect of this collection of information, including suggestions for reducing the burden, to Department of Defense, Washington Headquarters Services, Directorate for Information Operations and Reports (0704-0188), 1215 Jefferson Davis Highway, Suite 1204, Arlington, VA 22202-4302. Respondents should be aware that notwithstanding any other provision of law, no person shall be subject to any penalty for failing to comply with a collection of information if it does not display a currently valid OMB control number. PLEASE DO NOT RETURN YOUR FORM TO THE ABOVE ADDRESS.					
1. REPORT DATE (DD-MM-YYYY) August 2015		2. REPORT TYPE Final		3. DATES COVERED (From - To) December 2013–December 2014	
4. TITLE AND SUBTITLE High-Permeability Magnetic Polymer Additives for Lightweight Electromagnetic Shielding				5a. CONTRACT NUMBER	
				5b. GRANT NUMBER	
				5c. PROGRAM ELEMENT NUMBER	
6. AUTHOR(S) Kristen S Williams and B Christopher Rinderspacher				5d. PROJECT NUMBER MMSD-FY14-18	
				5e. TASK NUMBER	
				5f. WORK UNIT NUMBER	
7. PERFORMING ORGANIZATION NAME(S) AND ADDRESS(ES) US Army Research Laboratory ATTN: RDRL-WMM-G Aberdeen Proving Ground, MD 21005-5066				8. PERFORMING ORGANIZATION REPORT NUMBER ARL-TR-7372	
9. SPONSORING/MONITORING AGENCY NAME(S) AND ADDRESS(ES)				10. SPONSOR/MONITOR'S ACRONYM(S)	
				11. SPONSOR/MONITOR'S REPORT NUMBER(S)	
12. DISTRIBUTION/AVAILABILITY STATEMENT Approved for public release; distribution is unlimited.					
13. SUPPLEMENTARY NOTES					
14. ABSTRACT This report describes fundamental research on the magnetic properties of organometallic complexes and their performance as potential dopants in polymeric electromagnetic (EM) shielding materials. The research hypothesis was that ferromagnetic polymers can be realized via doping with magnetic organometallic complexes, and that the magnetic spin state of the dopant determines the bulk magnetic response. To test this hypothesis, the magnetic properties of several organometallic complexes were investigated using spin-polarized quantum chemistry calculations. It was found that organometallic complexes can have high spin states with large magnetic stabilization energies. The key chemical design principles for achieving high-spin dopants were identified, and the best performance was found in organometallic complexes containing Cr ²⁺ , Mn ²⁺ , and Fe ²⁺ bound to aromatic rings. A FORTRAN code to simulate the 3-dimensional Ising model was developed, and it revealed that ferromagnetic ordering in doped polymers is highly dependent on dopant distance and not possible for cases when complexes are widely dispersed. Nevertheless, polymeric matrices doped with high-spin complexes still exhibit a paramagnetic response to an external magnetic field and could enable the development of lightweight EM shielding materials. To guide future materials selection, this report concludes with a table of recommended complexes that have the best magnetic performance.					
15. SUBJECT TERMS magnetism, polymers, organometallic, quantum chemistry, Ising model					
16. SECURITY CLASSIFICATION OF:			17. LIMITATION OF ABSTRACT UU	18. NUMBER OF PAGES 44	19a. NAME OF RESPONSIBLE PERSON B Christopher Rinderspacher
a. REPORT Unclassified	b. ABSTRACT Unclassified	c. THIS PAGE Unclassified			19b. TELEPHONE NUMBER (Include area code) (410) 306-2811

Contents

List of Figures	iv
List of Tables	iv
1. Introduction	1
2. Literature Review	3
3. Computational Methods	4
4. Results and Discussion	6
4.1 Magnetic Properties of Organometallic Complexes	6
4.2 Magnetic Coupling in Dimer Models.....	8
4.3 Macroscopic Magnetic Properties from Classical Spin Models	9
5. Conclusions	12
6. Recommendations	12
7. References	14
Appendix. Supplementary Density Functional Theory (DFT) Data for All Investigated Complexes	19
List of Symbols, Abbreviations, and Acronyms	33
Distribution List	35

List of Figures

Fig. 1 Organic ligands considered in this study: [Cp] ⁻ = cyclopentadiene; [CHT] ⁺ = cycloheptatrienyl; [COT] ²⁻ = cyclooctatetraene.....	4
Fig. 2 ΔE_{mag} vs. Z for a series of half-sandwich organometallic complexes containing divalent metal cations. ΔE_{mag} values calculated with DFT using the PBE0 functional.....	6
Fig. 3 Optimized structures and spin state splittings for 3 selected organometallic complexes containing Fe ²⁺ cations. [Cp] = cyclopentadiene; [Py] = pyrrole; [Imid] = imidazole. ΔE_{mag} values calculated with DFT using the PBE0 functional.....	7
Fig. 4 ΔE_{mag} vs. $2S+1$ for a series of half-sandwich organometallic complexes containing a) different-sized C rings and b) 5-membered rings with different composition. ΔE_{mag} values calculated with DFT using the PBE0 functional.....	8
Fig. 5 (a) Dimer model for 2 FePyCl ₂ complexes separated by distance d . (b) J vs. d for dimer models of FePyCl ₂ and FePhCl ₂ . Positive J indicates ferromagnetic coupling between spins on adjacent complexes.....	9
Fig. 6 Plots of macroscopic thermodynamic variables computed for an interacting Ising model of 64,000 Fe atoms (assuming $J_{\text{Fe-Fe}} \approx 16$ meV): a) M vs. T at $B = 0$, b) C_V vs. T at $B = 0$, and c) M vs. T for varying values of B	10
Fig. 7 Plots of macroscopic thermodynamic variables computed for an interacting Ising model of 64,000 FePyCl ₂ complexes. J was taken to be 41 meV at $d = 0.5$ nm and 1.5 meV at $d = 1.0$ nm. a) M vs. T at $B = 0$ and b) C_V vs. T at $B = 0$	11
Fig. 8 Plots of M vs. T for varying values of B computed for an interacting Ising model of 64,000 FePyCl ₂ complexes separated by a) $d = 0.5$ nm and b) $d = 1.0$ nm. Red line corresponds to $B = 0$	11

List of Tables

Table 1 Relevant thermodynamic variables.....	5
Table 2 Top 40% of organometallic dopants considered in the study; ranking determined by strength of magnetic stabilization energy. Bold complexes have more than one high spin state.	13
Table A-1 Energy difference between high- and low-spin magnetic states in transition metal chlorides, M(x)Cl _x	20
Table A-2 Energy difference between high- and low-spin magnetic states in transition metal ion-cyclopentadiene (Cp ⁻) complexes.....	21

Table A-3	Energy difference between high- and low-spin magnetic states in transition metal ion-benzene (Ph) complexes	24
Table A-4	Energy difference between high- and low-spin magnetic states in transition metal ion- cycloheptatrienyl (Hp^+) complexes	26
Table A-5	Energy difference between high- and low-spin magnetic states in transition metal ion-cyclooctatetraene ($[\text{COT}]^{2-}$) complexes	27
Table A-6	Energy difference between high- and low-spin magnetic states in transition metal ion-pyrrole (Py) complexes.....	29
Table A-7	Energy difference between high- and low-spin magnetic states in transition metal ion-imidazole (Imid) complexes	30
Table A-8	Energy difference between high- and low-spin magnetic states in transition metal ion-thiophene (Thio) complexes	31

INTENTIONALLY LEFT BLANK.

1. Introduction

The interaction of materials with magnetic fields has a long history in US Army applications, such as magnetic shielding and ferromagnetically enhanced antennae, but also more recently in the processing of materials. These applications require conformable, thin, lightweight materials with high magnetic permeability, μ . Magnetic permeability is a macroscopic materials property defining how a bulk material responds to an external magnetic field [$\mathbf{B} = \mu \mathbf{H}$]. Effective magnetic shielding materials are characterized by 1) large values of relative magnetic permeability, μ_r , 2) resistance to local and global spin-state changes, and 3) isotropic response to an external magnetic field. Instead of blocking an impending magnetic field, high- μ_r materials create a path for field lines to be deflected around the shielded area. Anisotropy in μ_r complicates the behavior of shielding materials, as particular care has to be taken to ensure proper alignment with an external field.

Current commercial magnetic shielding materials contain mu-metals, which are a range of nickel-iron (Ni-Fe) alloys with high μ , but these materials are heavy, rigid, and costly. Furthermore, the current ferromagnetic material being used in Army antenna applications is a high- μ meta-ferrite.^{1,2} These materials are fabricated in limited sizes that may not be suitable for covering large curved surfaces of ground or air vehicles. Polymeric matrices, on the other hand, are highly conformable, flexible, and generally light. Polymers have densities around 1–2 g/cm³, while those of copper (Cu) and mu-metal are almost 9 g/cm³. Polymers can also be easily fabricated to any size and shape. By doping or choosing appropriate monomers, polymers can be manipulated to exhibit desired properties such as mechanical toughness or electrical conductivity.

Recent work has shown that adding magnetic particles to soft materials (carbonyl iron in polyurethane³ and magnetite in skin grafts,⁴ for example) changes their bulk response to a magnetic field. Doping conductive polyaniline (PANI) with magnetite particles (Fe₃O₄) creates a composite with saturation magnetization approximately 100 times that of the neat polymer.⁵ Physical incorporation of magnetic particles in polymer matrices is well established and can achieve the desired magnetic properties; however, this approach introduces polymer-ceramic interfaces that can cause poor dispersion and nonuniform shielding. As an example of a lightweight alternative, graphene can be made ferromagnetic by chemically bonding metal atoms (both high- and low-spin ions) onto the surface.⁶ Enhanced ferromagnetism in graphene can be elicited by intercalating the sheets with chromium (Cr) ions.⁷ Until now the emphasis has been on Cr-based organometallics because they readily sandwich between graphene layers⁸ and create linker groups between carbon nanotubes.⁹ A few recent computational and experimental works on organometallics bonded to graphene have been reported,^{10–12} but the general trend is for the metals' high-spin states to be quenched on the surface.

These recent reports on metal-dopant-induced magnetism in graphene are promising advancements for the synthesis of magnetic polymers. Polymers are generally closed-shell, purely organic materials (no metal content) with no net magnetic moment. Because polymers can be synthesized with aromatic carbon (C) rings, however, similar metal-induced magnetism should be possible. Furthermore, doping polymers with magnetic organometallic complexes may result in lightweight low-metal-content composites with good dispersion of dopants and a tunable magnetic response.

Prior research on magnetic properties of coordination complexes has focused on spintronics, molecular magnets, and quantum computing. In these applications, it is desirable to exhibit low spin-flip energies, i.e., decoupled individual spin states are close in energy, and the magnetic response has to be actively controlled and maintained via temperature, applied voltage, or laser pulses. In contrast, shielding applications require a passive resistance to local and global spin-state changes. More specifically, the following 3 factors determine the magnetic permeability of doped polymer systems:

- Spin state of the dopant: Relative magnetic permeability, μ_r , is related to spin state, S , through the equation

$$\mu_r - 1 = \frac{\mu_0 n g^2 \mu_b^2 (L+S)(L+S+1)}{3k_B T}, \quad (1)$$

where μ_0 is the permeability of free space, n is the concentration of free spins, g is the Landé g factor, μ_b is the Bohr magneton, L is the orbital angular momentum, k_B is the Boltzmann constant, and T is temperature. Since μ_r is linearly proportional to S , high spin states increase the interaction with an external magnetic field.

- Spin-state splitting of the dopant (or magnetic stabilization energy): This is the energy necessary to change the spin state. Large spin-state splitting prevents a decrease in spin state under a (low-frequency) magnetic field. A decrease in spin state is undesirable, as this would subsequently reduce the magnetic character of the dopant.
- Magnetic coupling, J , between dopants sitting on different sites within the polymer matrix: Positive J (ferromagnetic coupling) between dopants guarantees a constructive interference, which leads to high μ . The strength of J also determines the Curie temperature, above which spontaneous ferromagnetic ordering is lost due to thermal fluctuations.

This report describes fundamental research conducted to assess the potential for using organometallic dopants in polymeric shielding materials. The research hypothesis was that ferromagnetic polymers can be realized via doping with magnetic organometallic complexes and that the magnetic structure of the dopant determines the bulk magnetic response, i.e., magnetically doped polymeric matrices will exhibit high magnetic permeability and Curie

temperature (greater than room temperature). To test this hypothesis, the magnetic properties of several organometallic complexes were investigated using spin-polarized quantum chemistry calculations. Research focused on organometallic coordination complexes containing high-spin metal ions (Ni, Fe, manganese [Mn], etc.) bound to aromatic ligands with highly delocalized π -electrons, of which the polyacenes and graphene are limiting cases. Such systems have a rich number of magnetic states based on metal ion spin state, ligand chemistry, and the presence of counter ions.

This report describes findings related to the aforementioned key factors for high μ , namely, preferred spin states of the dopant complexes and energy splittings between different spin states. For selected complexes with high spin states, the magnetic coupling between dopants was evaluated with dimer models, and the computed magnetic coupling constants, J , were used as input for classical spin models. This enabled the prediction of macroscopic magnetic properties of the doped polymeric systems including magnetic susceptibility, χ (related to μ), and Curie temperature, T_C , as a function of dopant chemistry and dispersion (defined by dimer distance). This report concludes with recommendations for dopant selection and general comments on the feasibility of achieving ferromagnetic ordering in polymers.

2. Literature Review

The dopants of interest in the present work are half-sandwich organometallic complexes consisting of a single transition metal cation bonded to an aromatic ligand. Each complex contains a single metal atom, M , with charge $+x$, and a ligand, L , with charge y . Charge neutrality is imposed by adding an appropriate number of Cl^- counter ions to the metal, which generates stoichiometric structures of the general form $\text{M}^x\text{L}^y\text{Cl}_{x+y}$. Such dopants can be introduced to polymeric materials either by entrapment inside the polymer matrix (physical incorporation) or chemical incorporation as part of the polymer chain backbone or linked as pendant groups.¹³ Many transition-metal organometallic complexes are paramagnetic compounds with odd-electron counts and open-shell valence configurations.^{14,15} In these complexes, different spin configurations result from the distribution of unpaired valence electrons among d orbitals that have been split by the presence of a ligand field.¹⁶

The structures and magnetic properties of some transition metal half-sandwich complexes containing aromatic ligands have been reported previously. In the area of half-sandwich and sandwich complexes (i.e., those containing no more than one aromatic ligand), the most extensively studied ligands are cyclopentadienyl $[(\text{C}_5\text{H}_5)^-]$ ^{15,17–19} and benzene (C_6H_6) ,^{15,20–50} with only a few works devoted to cycloheptatrienyl $[(\text{C}_7\text{H}_7)^+]$,^{15,38,51} cyclo-octatetraene $[(\text{C}_8\text{H}_8)^{2-}]$,⁵² pyrrole (C_4NH_5) ,⁵³ and other heterocyclic ligands.^{36,54} The cyclopentadienyl ligand, in particular, is ubiquitous in organometallic chemistry and forms half-sandwich complexes with almost all

transition metal,⁵⁵ main-group,⁵⁶ and rare earth elements.⁵⁷ The structure and reactivity of paramagnetic organometallic compounds containing cyclopentadienyl are related to their spin state, and both high- and low-spin configurations can occur depending on the electron count.¹⁴

Transition metal half-sandwich complexes containing benzene also display unique magnetic structures. For example, Pandey et al.^{20,21} used density functional theory (DFT) to determine the geometries, energetics, and electronic structures of neutral and charged 3d transition metal atoms interacting with benzene. Metal-benzene half-sandwich complexes were studied with M^0 and M^+ charge states, and it was found that the spin states of scandium (Sc), titanium (Ti), and vanadium (V)-benzene complexes are enhanced while those of Mn-, Fe-, cobalt- (Co), and Ni-benzene complexes are reduced from their values in the free metal atom. Only the magnetic moment of the neutral Cr atom remains unchanged when bound to benzene. These findings show that the spin states (and resultant magnetic properties) of organometallic complexes can be tuned by the choice of metal-ligand composition.

3. Computational Methods

The organometallic complexes of interest were half-sandwich complexes consisting of organic ligands bonded to high-spin first-row transition metals. The metals considered were V, Cr, Mn, Fe, Co, and Ni, and these were bonded to a series of organic ligands containing aromatic C rings, as shown in Fig. 1. The ligands were chosen to probe the effects of both ring size (5–8 C atoms) and ring composition (e.g., substituting sulfur [S] for C in thiophene [Thio]) on the magnetic properties of the final complex.

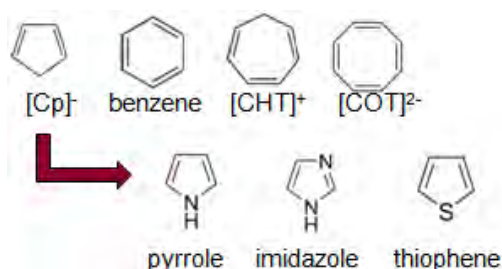


Fig. 1 Organic ligands considered in this study:
[Cp]⁻ = cyclopentadiene;
[CHT]⁺ = cycloheptatrienyl;
[COT]²⁻ = cyclooctatetraene.

All organometallic complexes were optimized using the NWCHEM quantum chemistry code,⁵⁸ and electronic energies were calculated with DFT at the PBE0/6-31G(d) level of theory.

The spin-state splitting, or magnetic stabilization energy, is defined as the energy difference between 2 spin states, as follows:

$$\Delta E_{mag} = E(S_{high}) - E(S_{low}). \quad (2)$$

From Eq. 2, negative stabilization energies indicate that high-spin magnetic ordering is more energetically favorable than low-spin ordering. Thus complexes with negative ΔE_{mag} prefer high spin states with the maximum number of unpaired valence electrons. Conversely, complexes with positive ΔE_{mag} prefer low spin configurations. If the preferred low spin state is exactly $S = 0$ (i.e., all valence electrons are paired), the complex prefers to be closed shell and will display a diamagnetic response to an applied field.

The magnetic coupling constant between 2 localized spins in a dimer model is defined by Barone et al.⁵⁹

$$J = \frac{E(S_{low}) - E(S_{high})}{S_{high}(S_{high} + 1)}. \quad (3)$$

According to convention, $J > 0$ indicates ferromagnetic exchange while $J < 0$ indicates antiferromagnetic exchange. This convention comes from the classical spin Hamiltonian, defined by Heisenberg⁶⁰ as

$$H = -J \sum_{i,j} s_i s_j - B \sum_i s_i, \quad (4)$$

where J is the magnetic coupling between nearest-neighbor spins, s_i , and B is the strength of the external field. With the defined spin Hamiltonian, the partition function of a fully interacting system of spins can be written as the following:

$$Q(B, T) = \sum_{s_1} \sum_{s_2} \cdots \sum_{s_N} e^{-\frac{H}{k_B T}}, \quad (5)$$

from which all subsequent thermodynamic variables can be computed, including heat capacity, magnetization, and magnetic susceptibility. Equations for relevant variables are listed in Table 1.

Table 1 Relevant thermodynamic variables

Thermodynamic Variable	Equation
Helmholtz free energy	$F(B, T) = -Nk_B T \ln Q(B, T)$
Heat capacity	$C_V = \left(\frac{\partial F}{\partial T} \right)_V$
Magnetization	$M(B, T) = - \left(\frac{\partial F}{\partial B} \right)_{V, T}$
Magnetic susceptibility	$\chi = \left(\frac{\partial M}{\partial B} \right)_T$

4. Results and Discussion

4.1 Magnetic Properties of Organometallic Complexes

Figure 2 shows the spin-state splittings, or magnetic stabilization energies, ΔE_{mag} , for organometallic complexes containing divalent metal cations. The energies were calculated with Eq. 2 and are plotted against atomic number of the metal cation. The spin states and corresponding DFT energies used to calculate ΔE_{mag} are provided as supplementary data in the Appendix. For comparison, stabilization energies calculated with only Cl^- ligands are also plotted in Fig. 2 (indicated with diamonds). ΔE_{mag} for different cations bonded to organic ligands spans a wide range from ± 80 kcal/mol. Complexes with large positive ΔE_{mag} have a strong preference for low spin states in which spins are paired. In contrast, complexes with negative ΔE_{mag} prefer high spin states with a majority of spins unpaired.

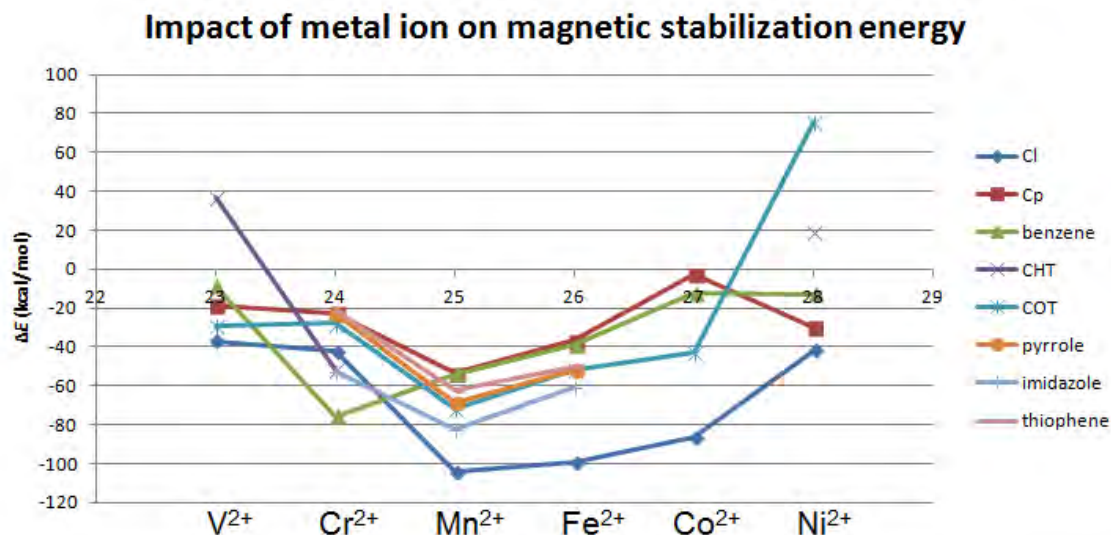


Fig. 2 ΔE_{mag} vs. Z for a series of half-sandwich organometallic complexes containing divalent metal cations. ΔE_{mag} values calculated with DFT using the PBE0 functional.

Figure 3 shows representative results for 3 magnetic complexes containing Fe^{2+} . This series compares the effects of ligand composition. Specifically, ΔE_{mag} for FeCpCl is -30 kcal/mol, indicating that this complex prefers a high spin state. ΔE_{mag} becomes stronger (decreases to -48 kcal/mol) when one C atom in the 5-membered ring is substituted with nitrogen (N) to form a pyrrole complex. The magnetic stabilization increases even more (ΔE_{mag} decreases to -56 kcal/mol) when a second C atom is substituted to form an imidazole complex. The increased magnetic stabilization results from electronic effects on the N atoms, and these results show that magnetism in half-sandwich complexes can be tailored by the choice of ligand.

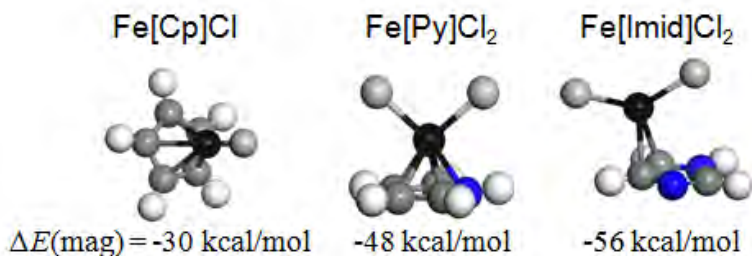


Fig. 3 Optimized structures and spin state splittings for 3 selected organometallic complexes containing Fe^{2+} cations. [Cp] = cyclopentadiene; [Py] = pyrrole; [Imid] = imidazole. ΔE_{mag} values calculated with DFT using the PBE0 functional.

The data in Fig. 2 enable a comparison of the magnetic character of different organic ligands. Specially, the largest spin-state splittings are observed for inorganic Cl^- ligands, while stabilization energies for organic ligands are comparable across the range of atomic numbers. One notable exception is the Cr^{2+} -benzene complex, which has a larger spin-state splitting than CrCl_2 . Aside from the Cr^{2+} -benzene complex, however, the largest stabilization energies are achieved with the Imid, Py, and $[\text{COT}]^{2-}$ ligands.

Aside from effects due to ligand, the choice of metal cation has a large impact on ΔE_{mag} . When comparing different metal ions, there are some clear trends in the data in Fig. 2. The first is that the strongest magnetic stabilization is achieved with Cr^{2+} , Mn^{2+} , and Fe^{2+} . This is an expected finding given that these cations have the largest number of unpaired d electrons. In contrast, V^{2+} , Co^{2+} , and Ni^{2+} display weaker, although still negative, spin-state splittings. This reveals that half-sandwich complexes containing V^{2+} , Co^{2+} , and Ni^{2+} can have high spin states but are less stabilized with respect to low spin states. Thus, high spin-state organometallic complexes containing Cr^{2+} , Mn^{2+} , and Fe^{2+} are more favorable for use in shielding applications because they will display increased interaction with an external magnetic field.

Another way to analyze the magnetic character of organometallic complexes is to compare ΔE_{mag} with the magnitude of the spin state, S . Figure 4 shows plots of ΔE_{mag} versus $2S+1$ for stable complexes having a) different sized C rings and b) different ligand composition. Plotting the data in this way reveals 2 key aspects of magnetic structure in half-sandwich complexes. First, high spin states (up to $2S+1 = 5$) and large magnetic stabilization energies are possible with ligands containing any size C ring. Also, substitution of C with N or S enhances the magnetic properties. Complexes with Py, Imid, and Thio tend to be stabilized at higher spin states ($S = 4, 5$) with larger values of ΔE_{mag} compared with the simple 5-membered C ring, Cp^- . Thus, these ligands should experience the largest interaction with an external field.

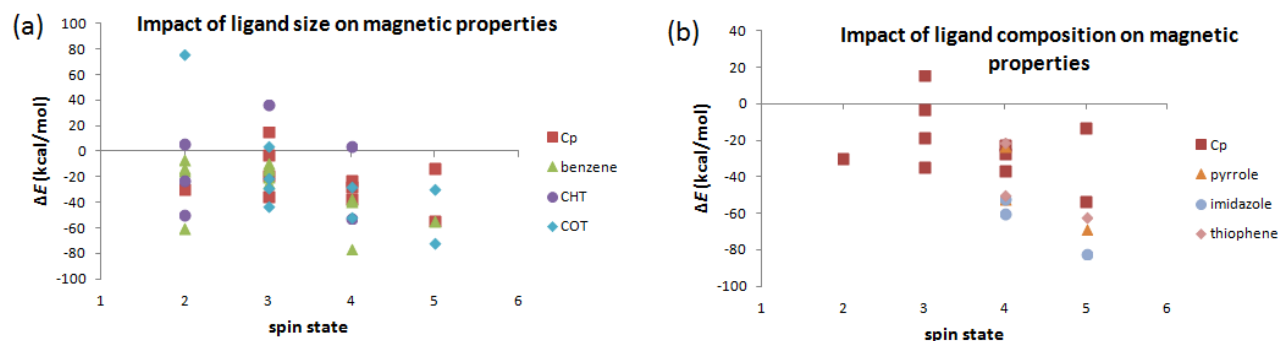


Fig. 4 ΔE_{mag} vs. $2S+1$ for a series of half-sandwich organometallic complexes containing a) different-sized C rings and b) 5-membered rings with different composition. ΔE_{mag} values calculated with DFT using the PBE0 functional.

4.2 Magnetic Coupling in Dimer Models

The magnetic coupling, J , between adjacent complexes with high spin states and large values of ΔE_{mag} was determined by developing dimer models and computing J with Eq. 3. Figure 5a shows a representative dimer model of 2 adjacent Fe^{2+} -Py complexes separated by distance d (measured between metal centers). Magnetic coupling was calculated at different dimer distances, and J versus d for dimers of both FePyCl_2 and FePhCl_2 is plotted in Fig. 5b. It is clear that magnetic exchange coupling is positive for these dimer systems, indicating ferromagnetic ordering at dimer distances of approximately 0.5–1.0 nm. However, J is only strong at small dimer distances and drops off sharply when the 2 complexes are separated by more than 1.0 nm. This suggests that ferromagnetic coupling between complexes on adjacent sites will be robust only at high dopant levels. If dopants are dispersed more widely, such that intercomplex distances are on the order of a few nanometers, magnetic coupling between complexes will be quenched unless other mechanisms for spin coupling are provided, such as conjugated polymer backbones. Unpaired electrons on complexes with high spin states will still interact with an external magnetic field, but self-interaction and the possibility for ferromagnetic ordering of spins will be negligible.

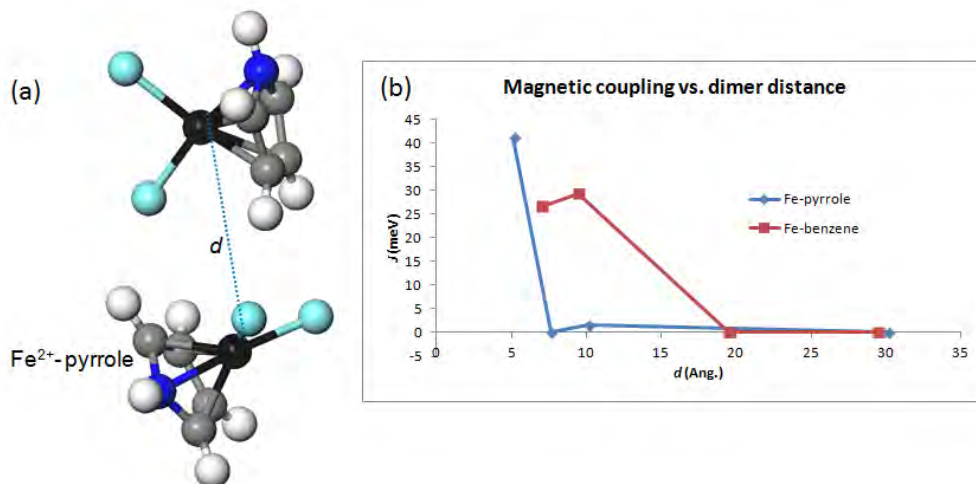


Fig. 5 (a) Dimer model for 2 FePyCl₂ complexes separated by distance d . (b) J vs. d for dimer models of FePyCl₂ and FePhCl₂. Positive J indicates ferromagnetic coupling between spins on adjacent complexes.

4.3 Macroscopic Magnetic Properties from Classical Spin Models

Using calculated values of the magnetic exchange interaction in dimer models, the macroscopic magnetic properties of a 3-dimensional (3-D) array of organometallic complexes are calculated using the Hamiltonian in Eq. 4. The Hamiltonian is solved for a 3-D Ising model of 64,000 spins using a Monte Carlo FORTRAN code. The code was validated by computing magnetization, M , and heat capacity, C_V , as a function of temperature for an array of interacting Fe atoms ($J_{\text{Fe-Fe}} \approx 16 \text{ meV}$)⁶¹ under zero applied field ($B = 0$). Figure 6 shows plots of M versus T and C_V versus T for an array of Fe atoms. As expected, the Ising model predicts ferromagnetic ordering and finite magnetization at low temperatures (Fig. 6a). Ordering of spins due to magnetic self-interaction weakens at elevated temperatures, as increasing entropy drives spins to fluctuate randomly. Above a characteristic temperature—the Curie temperature, T_C —spin ordering is completely destroyed and net magnetization drops to zero around 1,000 K. This is consistent with Fe's ferromagnetic-to-paramagnetic phase transition at $T_C = 1,043 \text{ K}$. The exact value of T_C predicted by the Ising model can be estimated from the plot of C_V versus T in Fig. 6b. Because ferromagnetic-to-paramagnetic phase transitions are second-order phase transitions, heat capacity diverges at the Curie point. The predicted value of T_C from Fig. 6b is 850 K, which is fairly close to the experimental value of 1,043 K. The value of T_C for bulk Fe is underestimated in this spin model because the chosen Hamiltonian only accounts for magnetic coupling between nearest neighbors. While this is a slight source of error for bulk Fe (magnetic coupling can occur between the second and third nearest neighbors), it is a reasonable approximation for an array of organometallic spins given that J drops off sharply as a function of spin separation (see Fig. 5b). Figure 6c shows a plot of M versus T for the same array of Fe atoms but with increasing magnitude of applied magnetic field, B . The data points in Fig. 6c can be used to calculate the magnetic susceptibility, χ , by taking the derivative of M with respect to B at a fixed value of T (see equation for χ in Table 1).

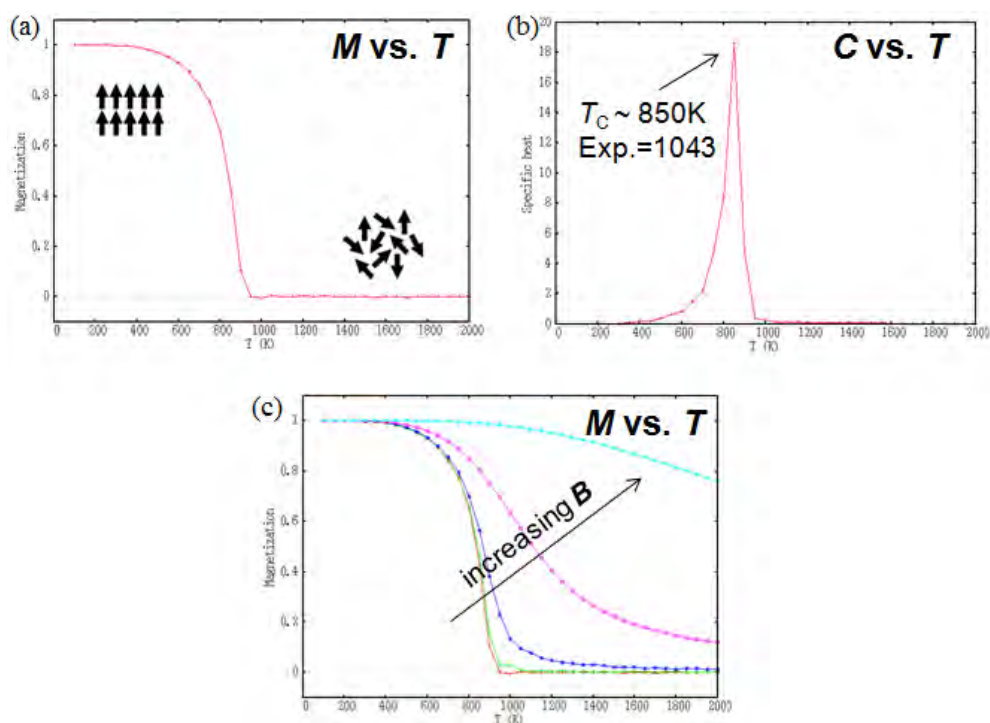


Fig. 6 Plots of macroscopic thermodynamic variables computed for an interacting Ising model of 64,000 Fe atoms (assuming $J_{\text{Fe-Fe}} \approx 16$ meV): a) M vs. T at $B = 0$, b) C_V vs. T at $B = 0$, and c) M vs. T for varying values of B

The Ising model was subsequently applied to a system of interacting organometallic complexes; specifically, thermodynamic variables were computed for an array of 64,000 FePyCl₂ complexes separated by Fe-Fe interatomic distances of 0.5 and 1.0 nm. Plots of relevant variables (at $B = 0$) are shown in Fig. 7. The predicted Curie temperature for a matrix of FePyCl₂ complexes separated by 0.5 nm is 2,100 K, which is much higher than that of bulk Fe because of the enhanced magnetic coupling interaction, $J \approx 41$ meV. In a real polymer matrix, however, it is expected that dopant loadings will not be so dense or well-ordered. As shown in Fig. 5b, the magnetic coupling drops sharply at large dimer separations, so it is expected that self-interactions will be insignificant at sparse loading levels. Therefore, assuming a small value of $J \approx 1.5$ meV at $d = 1.0$ nm, it is found that the same array of 64,000 FePyCl₂ complexes displays no spontaneous ordering of spins and effectively zero magnetization at all temperatures.

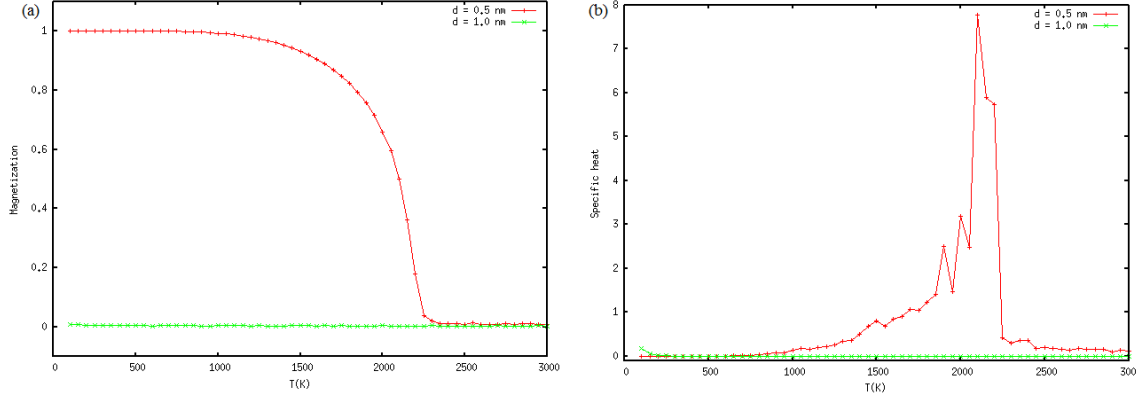


Fig. 7 Plots of macroscopic thermodynamic variables computed for an interacting Ising model of 64,000 FePyCl₂ complexes. J was taken to be 41 meV at $d = 0.5$ nm and 1.5 meV at $d = 1.0$ nm. a) M vs. T at $B = 0$ and b) C_V vs. T at $B = 0$.

Quantum chemistry calculations show that magnetic self-interactions between widely dispersed complexes ($d > 1.0$ nm) are quenched. However, complexes with high spin states will still interact with an external magnetic field. This is shown in Fig. 8, which contains plots of M versus T for organometallic arrays subjected to applied magnetic fields of varying strength. As shown in Fig. 8b, the net magnetization of an array of organometallic complexes separated by 1.0 nm is effectively zero at $B = 0$ (red line). However, finite magnetization can be induced at low temperatures (i.e., room temperature) by applying increasingly stronger magnetic fields. Thus, polymers doped with magnetic organometallic complexes will display paramagnetic behavior in an external magnetic field even if dopants are widely dispersed. Under these conditions, the spins will not interact with each other and will be “free spins”, responding only to thermal fluctuations and external magnetic fields.

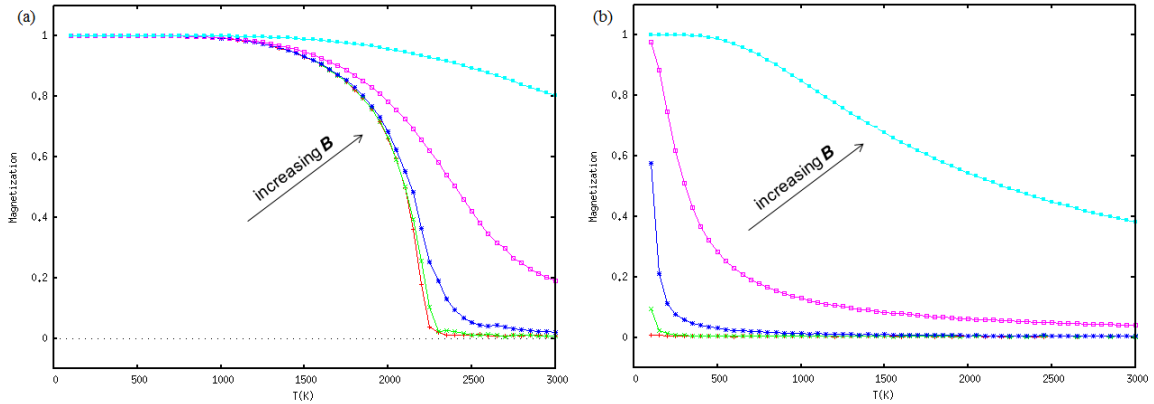


Fig. 8 Plots of M vs. T for varying values of B computed for an interacting Ising model of 64,000 FePyCl₂ complexes separated by a) $d = 0.5$ nm and b) $d = 1.0$ nm. Red line corresponds to $B = 0$.

5. Conclusions

Spin-polarized quantum chemistry calculations were used to determine the structure and magnetic ordering in a large number of half-sandwich organometallic complexes. Calculations validated one of the underlying hypotheses, which was that organometallic complexes can have high spin states with large magnetic stabilization energies. Key chemical design principles for achieving high-spin dopants were identified; specifically, the highest spin states and largest magnetic energies are achievable in dopants with Cr^{2+} , Mn^{2+} , and Fe^{2+} bound to aromatic rings. Moreover, rings substituted with N and S (Py, Imid, and Thio) display even stronger magnetic character due to electronic effects on the ligand. Dimer models were developed for complexes having the largest spin states, and magnetic coupling, J , was computed as a function of metal-metal interatomic distance. It was found that magnetic exchange at small dimer distances ($\sim 0.5\text{--}1.0$ nm) is large and positive, indicating ferromagnetic ordering. However, J quickly drops to zero when complexes are separated by more than 1.0 nm, which is likely to occur when dopants are dispersed in a polymer matrix. Thus, one of the starting hypotheses—namely that ferromagnetic character could be induced in polymers—was found to be highly dependent on dopant distance and not possible for cases when complexes are widely dispersed.

A FORTRAN code was developed to simulate a 3-D classical Ising spin model. This code was validated for an array of interacting iron spins (to mimic bulk Fe) and was used to estimate Curie temperature and magnetic field response for doped polymeric systems. One of the key findings was that doped polymeric systems will behave as paramagnets in the presence of an external magnetic field even if magnetic self-interactions are negligible, as would be the case when dopants are widely dispersed. This indicates that lightweight electromagnetic shielding could be achievable with polymeric materials doped with magnetic organometallic complexes even if ferromagnetism is not feasible. Beyond this material system, however, the developed FORTRAN code is applicable to any system of magnetic spins (polymer, metal, ceramic, composite, etc.) and could be used to evaluate the behavior of a variety of materials under external magnetic field.

6. Recommendations

Based on the results of this investigation, a table of recommended dopants was developed both to highlight the key chemical design principles and to guide future materials selection. Table 2 lists the top 40% of organometallic dopants based on magnetic performance. All of these dopants have high spin states with large values of ΔE_{mag} and will therefore have strong interaction with an external magnetic field. Dopants in bold text are especially promising because they have more

than one favorable high spin state (i.e., $\Delta E_{\text{mag}} < 0$ for multiple values of S). These are good candidates for electromagnetic shielding because unpaired spins would align with the magnetic component of the field, and spin state flipping could provide a damping mechanism.

Table 2 Top 40% of organometallic dopants considered in the study; ranking determined by strength of magnetic stabilization energy. Bold complexes have more than one high spin state.

Top 40%			
Top 30%			...
Top 20%	
Top 10%
Mn(Imid)Cl ₂	FeHpCl₃	MnCpCl	[Fe(Thio)] ²⁺
[Fe(Imid)] ²⁺	MnPyCl ₂	CoHpCl₃	[MnPhCl₃]²⁺
[MnCp] ⁺	[MnPhCl₃]²⁻	Cr(Imid)Cl ₂	[FePy] ²⁺
CrPhCl₂	Mn(Thio)Cl ₂	FePyCl₂	[FePyCl] ⁺
[Fe(Imid)Cl] ⁺	Fe(Imid)Cl ₂	CrHpCl₃	[VCp] ⁺
MnHpCl₃	[CrHpCl ₃] ⁺	Fe(COT)	Co(COT)
Mn(COT)	MnPhCl₂	Fe(Thio)Cl ₂	[Fe(Thio)Cl] ⁺

7. References

1. Walser RM, Valanju AP. Displacement eddy currents in magnetic laminates. *IEEE Transactions on Magnetics*. 1992;28(5):2280–2282.
2. Walser RM, Valanju AP. GHz ferromagnetic resonances in laminated microscale objects. *Journal of Applied Physics*. 1997;81(8):5169–5169.
3. Mitumata T, Ohori S, Honda A, Kawai M. Magnetism and viscoelasticity of magnetic elastomers with wide range modulation of dynamic modulus. *Soft Matter*. 2013;9(3):904–912.
4. Ito A, Kamihira M. Tissue engineering using magnetite nanoparticles. In: Antonio V, editor. *Progress in molecular biology and translational science*. Amsterdam (The Netherlands): Academic Press; 2011. p. 355–395.
5. Saini P, Choudhary V, Vijayan N, Kotnala RK. Improved electromagnetic interference shielding response of poly(aniline)-coated fabrics containing dielectric and magnetic nanoparticles. *The Journal of Physical Chemistry C*. 2012;116(24):13403–13412.
6. Rotenberg E. The electronic properties of adsorbates on graphene. In: Raza H, editor. *Graphene nanoelectronics*. Berlin (Germany): Springer; 2012. p. 93–134.
7. Bui VQ, Le HM, Kawazoe Y, Nguyen-Manh D. Graphene-chromium-graphene intercalation nanostructures: stability and magnetic properties from density functional theory investigations. *The Journal of Physical Chemistry C*. 2013;117(7):3605–3614.
8. Kaloni TP, Kahaly MU, Schwingenschlogl U. Induced magnetism in transition metal intercalated graphitic systems. *Journal of Materials Chemistry*. 2011;21(46):18681–18685.
9. Bekyarova E, Sarkar, S, Wang F, Itkis ME, Kalinina I, Tian X, Haddon RC. Effect of covalent chemistry on the electronic structure and properties of carbon nanotubes and graphene. *Accounts of Chemical Research*. 2012;46(1):65–76.
10. Avdoshenko SM, Ioffe IN, Cuniberti G, Dunsch L, Popov AA. Organometallic complexes of graphene: toward atomic spintronics using a graphene web. *ACS Nano*. 2011;5(12):9939–9949.
11. Zhang YH, Zhou KG, Xie KF, Zhang HL, Peng Y, Wang CW. Tuning the magnetic and transport properties of metal adsorbed graphene by co-adsorption with 1,2-dichlorobenzene. *Physical Chemistry Chemical Physics*. 2012;14(33):11626–11632.

12. Zhang Z, Turner CH. Structural and electronic properties of carbon nanotubes and graphenes functionalized with cyclopentadienyl–transition metal complexes: a DFT study. *The Journal of Physical Chemistry C*. 2013;117(17):8758–8766.
13. Vorotyntsev MA, Vasilyeva SV. Metallocene-containing conjugated polymers. *Advances in Colloid and Interface Science*. 2008;139(1–2):97–149.
14. Leznoff DB, Hayes CE, Mund G. Paramagnetic organometallic complexes. In: *Encyclopedia of inorganic and bioinorganic chemistry*. Online. Hoboken (NJ): Wiley and Sons; 2006. DOI: 10.1002/9781119951438.
15. Poli R. Open-shell organometallics as a bridge between Werner-type and low-valent organometallic complexes: the effect of the spin state on the stability, reactivity, and structure. *Chemical Reviews*. 1996;96(6):2135–2204.
16. Alvarez S, and Cirera J. How high the spin? Allowed and forbidden spin states in Transition-metal chemistry. *Angewandte Chemie International Edition*. 2006;45(19):3012–3020.
17. Kemnitz CR, Ball ES, McMahon RJ. Photochemistry of CpMn(CO)_3 and related derivatives: spectroscopic observation of singlet and triplet CpMn(CO)_2 . *Organometallics*. 2011;31(1):70–84.
18. Snee PT, Payne CK, Kotz KT, Yang H, Harris CB. Triplet organometallic reactivity under ambient conditions: an ultrafast UV pump/IR probe study. *Journal of the American Chemical Society*. 2001;123(10):2255–2264.
19. Veiros LF. Haptotropic shifts in cyclopentadienyl organometallic complexes: ring folding vs. ring slippage. *Organometallics*. 2000;19(26):5549–5558.
20. Pandey R, Rao BK, Jena P, Blanco MA. Electronic structure and properties of transition metal–benzene complexes. *Journal of the American Chemical Society*. 2001;123(16):3799–3808.
21. Pandey R, Rao BK, Jena P, Newsam JM. Unique magnetic signature of transition metal atoms supported on benzene. *Chemical Physics Letters*. 2000;321(1–2):142–150.
22. Bauschlicher CW, Partridge H, Langhoff SR. Theoretical study of transition-metal ions bound to benzene. *The Journal of Physical Chemistry*. 1992;96(8):3273–3278.
23. Kandalam AK, Rao BK, Jena P, Pandey R. Geometry and electronic structure of $\text{V}_n(\text{Bz})_m$ complexes. *The Journal of Chemical Physics*. 2004;120(22):10414–10422.
24. Sohnlein BR, Li S, Yang DS. Electron-spin multiplicities and molecular structures of neutral and ionic scandium-benzene complexes. *The Journal of Chemical Physics*. 2005;123(21):214306–214312.

25. Polestshuk PM, Dem'yanov PI, Ryabinkin IG. The electronic structure and energetics of v^+ -benzene half-sandwiches of different multiplicities: comparative multireference and single-reference theoretical study. *The Journal of Chemical Physics*. 2008;129(5):054307.
26. Jaeger TD, van Heijnsbergen D, Klippenstein SJ, von Helden G, Meijer G, Duncan MA. Vibrational spectroscopy and density functional theory of transition-metal ion-benzene and dibenzene complexes in the gas phase. *Journal of the American Chemical Society*. 2004;126(35):10981–10991.
27. Kolakkandy S, Pratihari S, Aquino AJA, Wang H, Hase WL. Properties of complexes formed by Na^+ , Mg^{2+} , and Fe^{2+} binding with benzene molecules. *The Journal of Physical Chemistry A*. 2014;118(40):9500–9511.
28. Horváthová L, Dubecký M, Mitas L, Štich I. Quantum Monte Carlo study of π -bonded transition metal organometallics: neutral and cationic vanadium-benzene and cobalt-benzene half sandwiches. *Journal of Chemical Theory and Computation*. 2012;9(1):390–400.
29. Maynez-Rojas M, Castro M. Theoretical study of neutral and charged $Sc_{n \leq 2}-(benzene)_{m \leq 3}$ clusters. *Journal of Nanoparticle Research*. 2012;15(1):1–17.
30. Li H, Li C, Fan H, Yang J. Studies on electronic structures, energetics, and electron affinities of transition metal-benzene complexes and their anions with density functional theory. *Journal of Molecular Structure: THEOCHEM*. 2010;952(1–3):67–73.
31. Valencia I, Castro M. Theoretical study of the structural and electronic properties of the $Fe_n(C_6H_6)_m$, $n \leq 2$; $m \leq 2$ complexes. *Physical Chemistry Chemical Physics*. 2010;12(27):7545–7554.
32. Shao P, Kuang XY, Ding LP. Probing the structural, bonding, and magnetic properties of cobalt coordination complexes: co-benzene, co-pyridine, and co-pyrimidine. *The Journal of Physical Chemistry A*. 2013;117(48):12998–13008.
33. Zhang G, Wang W, Chen D. Chemical origin of blue and red shifts of C–H stretching vibrations in $M^+-C_2H_2$ ($M = V, Fe, Co, Ni$) and $M^+-C_6H_6$ ($M = V, Si, Ni$) complexes. *Chemical Physics*. 2008;354(1–3):225–229.
34. Wang J, Zhu L, Zhang X, Yang M. Size- and shape-dependent polarizabilities of sandwich and rice-ball CO_nBZ_m clusters from density functional theory. *The Journal of Physical Chemistry A*. 2008;112(36):8226–8230.
35. Zhang X, Wang J. Structural, electronic, and magnetic properties of $co_n(benzene)_m$ complexes. *The Journal of Physical Chemistry A*. 2007;112(2):296–304.
36. Mahadevi AS, Sastry GN. Cation- π interaction: its role and relevance in chemistry, biology, and material science. *Chemical Reviews*. 2012;113(3):2100–2138.

37. Horváthová L, Dubecký M, Mitas L, Štich I. Spin multiplicity and symmetry breaking in vanadium-benzene complexes. *Physical Review Letters*. 2012;109(5):053001.
38. Stanghellini PL, Diana E, Arrais A, Rossin A, Kettle SFA. Benzene and tropilium metal complexes. Intra- and intermolecular interaction evidenced by vibrational analysis: the blue-shift hydrogen bond. *Organometallics*. 2006;25(21):5024–5030.
39. Szczepanski J, Wang H, Vala M, Tielens AGGM, Eyler JR, Oomens J. Infrared spectroscopy of gas-phase complexes of Fe^+ and polycyclic aromatic hydrocarbon molecules. *The Astrophysical Journal*. 2006;646(1):666.
40. Béchamp K, Levesque M, Joly H, Manceron L. A combined electron paramagnetic resonance and Fourier transform infrared study of the $\text{Co}(\text{C}_6\text{H}_6)_{1,2}$ complexes isolated in neat benzene or in cryogenic matrixes. *The Journal of Physical Chemistry A*. 2006;110(18):6023–6031.
41. Jaeger TD, Duncan MA. Vibrational spectroscopy of $\text{Ni}^+(\text{benzene})_n$ complexes in the gas phase. *The Journal of Physical Chemistry A*. 2005;109(15):3311–3317.
42. Rabilloud F. Geometry and spin-multiplicity of half-sandwich type transition-metal-benzene complexes. *The Journal of Chemical Physics*. 2005;122(13):134303.
43. Duncan MA. Structures, energetics and spectroscopy of gas phase transition metal ion-benzene complexes. *International Journal of Mass Spectrometry*. 2008;272(2–3):99–118.
44. Ouhlal A, Selmani A, Yelon A. Bonding in $(\eta^6\text{-C}_6\text{H}_6) \text{M}$ and $(\eta^6\text{-C}_6\text{H}_6) \text{M}^+$, $\text{M} = \text{Ti}, \text{Cr}, \text{Ni}$, and Cu . A local spin density study. *Chemical Physics Letters*. 1995;243(3–4):269–274.
45. Yang CN, Klippenstein SJ. Theory and modeling of the binding in cationic transition-metal-benzene complexes. *The Journal of Physical Chemistry A*. 1999;103(8):1094–1103.
46. Gapeev A, Dunbar R. Reactivity and binding energies of transition metal halide ions with benzene. *Journal of the American Society for Mass Spectrometry*. 2002;13(5):477–484.
47. van Heijnsbergen D, von Helden G, Meijer G, Maitre P, Duncan MA. Infrared spectra of gas-phase $\text{V}^+(\text{benzene})$ and $\text{V}^+(\text{benzene})_2$ complexes. *Journal of the American Chemical Society*. 2002;124(8):1562–1563.
48. Chaquin P, Costa D, Lepetit C, Che M. Structure and bonding in a series of neutral and cationic transition metal–benzene η^6 complexes $[\text{M}(\eta^6\text{-C}_6\text{H}_6)]^{n+}$ ($\text{M} = \text{Ti}, \text{V}, \text{Cr}, \text{Fe}, \text{Co}, \text{Ni}$, and Cu). Correlation of charge transfer with the bathochromic shift of the e_1 ring vibration. *The Journal of Physical Chemistry A*. 2001;105(18):4541–4545.
49. Klippenstein SJ, Yang CN. Density functional theory predictions for the binding of transition metal cations to pi systems: from acetylene to coronene and tribenzocyclyne. *International Journal of Mass Spectrometry*. 2000;201(1–3):253–267.

50. Diefenbach M, Trage C, Schwarz H. Interactions of atomic iron cation with pyridine and benzene: a theoretical study on an unresolved controversy of bond energies and electronic ground-state structures. *Helvetica Chimica Acta*. 2003;86(4):1008–1025.
51. Green MLH, Ng DKP. Cycloheptatriene and -enyl complexes of the early transition metals. *Chemical Reviews*. 1995;95(2):439–473.
52. Lee JS, Lei Y, Kumari S, Yang D-S. Metal coordination converts the tub-shaped cyclo-octatetraene into an aromatic molecule: electronic states and half-sandwich structures of group III metal-cyclo-octatetraene complexes. *The Journal of Chemical Physics*. 2009;131(10):104304–104310.
53. Gapeev A, Yang C-N, Klippenstein SJ, Dunbar RC. Binding energies of gas-phase metal ions with pyrrole: experimental and quantum chemical results. *The Journal of Physical Chemistry A*. 2000;104(14):3246–3256.
54. Grimm RL, Mangrum JB, Dunbar RC. Complexation of gas-phase metal ions with furan: experimental and quantum chemical binding energies. *The Journal of Physical Chemistry A*. 2004;108(49):10897–10905.
55. O'Connor JM, Casey CP. Ring-slippage chemistry of transition metal cyclopentadienyl and indenyl complexes. *Chemical Reviews*. 1987;87(2):307–318.
56. Jutzi P, Burford N. Structurally diverse π -cyclopentadienyl complexes of the main group elements. *Chemical Reviews*. 1999;99(4):969–990.
57. Arndt S, Okuda J. Mono (cyclopentadienyl) complexes of the rare-earth metals. *Chemical Reviews*. 2002;102(6):1953–1976.
58. Valiev M, Bylaska EJ, Govind N, Kowalski K, Straatsma TP, Van Dam HJJ, Wang D, Nieplocha J, Apra E, Windus TL, de Jong WA. NWChem: A comprehensive and scalable open-source solution for large scale molecular simulations. *Computer Physics Communications*. 2010;181(9):1477–1489.
59. Barone V, Bencini A, di Matteo A. Intrinsic and environmental effects in the structure and magnetic properties of organic molecular magnets: bis(imino)nitroxide. *Journal of the American Chemical Society*. 1997;119(44):10831–10837.
60. Heisenberg, W. Mehrkörperproblem und Resonanz in der Quantenmechanik. *Zeitschrift für Physik*. 1926;38(6-7):411-426.
61. Camley RE, Tilley DR. Phase transitions in magnetic superlattices. *Physical Review B*. 1988;37(7):3413–3421.

Appendix. Supplementary Density Functional Theory (DFT) Data for All Investigated Complexes

This appendix appears in its original form, without editorial change.

Table A-1 Energy difference between high- and low-spin magnetic states in transition metal chlorides, $M(x)Cl_x$

Metal Ion	Complex	DFT Functional	Spin State, $2S+1$	E (Hartree)	ΔE_{mag} (kcal/mol)
V(II)	VCl ₂	PBE0	1	−1863.811784	−37.06
			3	−1863.870844	
		B3LYP	1	−1864.377554	−30.69
			3	−1864.426461	
Cr(III)	CrCl ₃	PBE0	1	−2424.332334	−43.43
			3	−2424.401542	
Cr(II)	CrCl ₂	PBE0	2	−1964.254623	−42.40
			4	−1964.322197	
		B3LYP	2	−1964.829477	−33.73
			4	−1964.883224	
Mn(II)	MnCl ₂	PBE0	2	−2070.69748	−45.05
			4	−2070.76927	
			6	−2070.86407	−104.54
Fe(III)	FeCl ₃	PBE0	2	−2643.46742	−42.02
			4	−2643.53439	
Fe(II)	FeCl ₂	PBE0	0	−2183.344986	−99.57
			4	−2183.503658	
		B3LYP	0	−2183.944312	−89.06
			4	−2184.086235	
Co(II)	CoCl ₂	PBE0	1	−2302.37808	−86.51
			3	−2302.51595	
		B3LYP	1	−2302.981534	−82.73
			3	−2303.113368	
Ni(II)	NiCl ₂	PBE0	0	−2427.92927	−41.72
			2	−2427.995758	
		B3LYP	0	−2428.54387	+67.47
			2	−2428.43635	

Table A-2 Energy difference between high- and low-spin magnetic states in transition metal ion-cyclopentadiene (Cp⁻) complexes

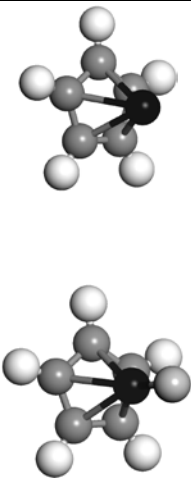
Metal Ion	Complex	Structure	DFT Functional	Spin State, 2S+1	<i>E</i> (Hartree)	ΔE_{mag} (kcal/mol)
V(II)	[VCp] ⁺	...	PBE0	1	-1136.701991	-43.22
				3	-1136.770867	
			B3LYP	1	-1137.126625	-54.41
				3	-1137.21334	
			HSE03	1	-1136.847159	-56.14
				3	-1136.936618	
	VCpCl		PBE0	1	-1597.108851	-18.43
				3	-1597.138226	
			B3LYP	1	-1597.723788	-16.33
				3	-1597.749817	
			HSE03	1	-1597.323879	-17.86
				3	-1597.352335	
Cr(III)	CrCpCl ₂	...	PBE0	1	-2157.61735	-34.48
				3	-2157.672298	
Cr(II)	[CrCp] ⁺	...	PBE0	2	-1237.155921	-32.63
				4	-1237.207925	
			B3LYP	2	-1237.611922	-29.28
				4	-1237.65859	
			HSE03	2	-1237.325575	-31.14
				4	-1237.375202	
			PBE0	2	-1697.535063	-22.50
				4	-1697.570923	
			B3LYP	2	-1698.162769	-17.19
				4	-1698.190164	
			HSE03	2	-1697.751124	-21.98
				4	-1697.786148	
Mn(II)	[MnCp] ⁺		HF	1	-1341.808401	-88.55
				5	-1341.949512	
			PBE0	1	-1343.598338	-77.66
				5	-1343.722092	
			B3LYP	1	-1344.067243	-69.71
				5	-1344.178329	
			HSE03	1	-1343.770882	-74.53
				5	-1343.889657	
			HF	1	-1801.650062	-89.08
				5	-1801.792018	
			PBE0	1	-1804.009078	-53.70
				5	-1804.094656	
			B3LYP	1	-1804.64944	-43.69
				5	-1804.719071	
			HSE03	1	-1804.228008	-51.37
				5	-1804.309877	

Table A-2 Energy difference between high- and low-spin magnetic states in transition metal ion-cyclopentadiene (Cp⁻) complexes (continued)

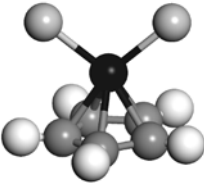
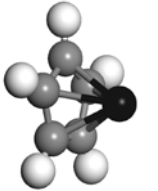
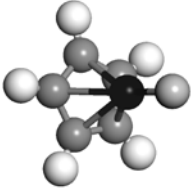
Metal Ion	Complex	Structure	DFT Functional	Spin State, 2S+1	E (Hartree)	ΔEmag (kcal/mol)
Mn(I)	MnCp	...	PBE0	2 4	-1343.849134 -1343.892971	-27.51
Fe(III)	[FeCp] ²⁺		HF	1 5	-- -1454.087276	-7.31
			PBE0	1 5	-1455.859648 -1455.871298	
			B3LYP	1 5	-1456.343277 -1456.346795	
			HSE03	1 5	-1456.036247 -1456.047116	
			HF	1 5	-1914.015069 -1914.090913	
			PBE0	1 5	-1916.401864 -1916.449942	
	[FeCpCl] ⁺		B3LYP	1 5	-- -1917.091622	-47.59
			HSE03	1 5	-1916.658037 -1916.673819	
			HF	1 5	-- -2373.917495	
			PBE0	1 5	-2376.788636 -2376.809397	
			B3LYP	1 5	-2377.60434 -2377.616655	
			HSE03	1 5	-2377.060353 -2377.080877	
	FeCpCl ₂		HF	1 5	-- -2373.917495	-9.90
			PBE0	1 5	-2376.788636 -2376.809397	
			B3LYP	1 5	-2377.60434 -2377.616655	
			HSE03	1 5	-2377.060353 -2377.080877	
			HF	1 5	-- -2373.917495	
			PBE0	1 5	-2376.788636 -2376.809397	
Fe(II)	[FeCp] ⁺		HF	0 4	-1454.445351 -1454.527657	-51.65
			PBE0	0 4	-1456.318156 -1456.371941	
			B3LYP	0 4	-1456.800703 -1456.844734	
			HSE03	0 4	-1456.491531 -1456.542533	
			HF	0 4	-1914.284108 -1914.383227	
			PBE0	0 4	-1916.690788 -1916.749366	
	FeCpCl		B3LYP	0 4	-1917.342553 -1917.389757	-36.76
			HSE03	0 4	-1916.911793 -1916.967178	
			HF	0 4	-1914.284108 -1914.383227	
			PBE0	0 4	-1916.690788 -1916.749366	
			B3LYP	0 4	-1917.342553 -1917.389757	
			HSE03	0 4	-1916.911793 -1916.967178	

Table A-2 Energy difference between high- and low-spin magnetic states in transition metal ion-cyclopentadiene (Cp⁻) complexes (continued)

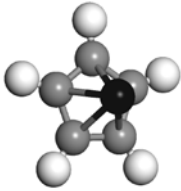
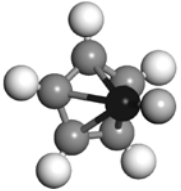
Metal Ion	Complex	Structure	DFT Functional	Spin State, 2S+1	E (Hartree)	ΔEmag (kcal/mol)
Co(II)	[CoCp] ⁺	...	PBE0	1	-1575.364936	4.51
				3	-1575.357752	
			B3LYP	1	-1575.85711	7.29
				3	-1575.845496	
			HSE03	1	-1575.544735	9.13
				3	-1575.530186	
	CoCpCl	...	PBE0	1	-2035.734083	-2.68
				3	-2035.738356	
			B3LYP	1	-2036.393756	0.36
				3	-2036.393183	
			HSE03	1	--	0.36
				3	-2035.957733	
Ni(III)	NiCpCl ₂	...	PBE0	1	-2621.315467	15.49
				3	-2621.290785	
Ni(II)	[NiCp] ⁺		HF	0	-1698.895451	-25.53
				2	-1698.936136	
			PBE0	0	-1700.856128	-25.55
				2	-1700.896852	
			B3LYP	0	-1701.361268	-22.26
				2	-1701.396748	
	NiCpCl		HSE03	0	-1701.031379	-24.78
				2	-1701.070874	
			HF	0	-2158.745278	-26.16
				2	-2158.786974	
			PBE0	0	-2161.222378	-29.62
				2	-2161.269587	
			B3LYP	0	-2161.893686	-27.12
				2	-2161.936897	
			HSE03	0	-2161.444688	-28.80
				2	-2161.490578	

Table A-3 Energy difference between high- and low-spin magnetic states in transition metal ion-benzene (Ph) complexes

Metal Ion	Complex	DFT Functional	Spin State, 2S+1	E (Hartree)	ΔE_{mag} (kcal/mol)
V(II)	[VPhCl ₃] ⁻	PBE0	2	-2556.01914	-14.44
			4	-2556.04215	
V(II)	VPhCl ₂	PBE0	2	-2095.87438	-8.82 65.15
			4	-2095.88844	
			6	-2095.77056	
V(IV)	[VPhCl ₃] ⁺	PBE0	2	-2555.67583	26.50
			4	-2555.6336	
V(V)	[VPhCl ₃] ²⁺	PBE0	1	-2555.1926	19.85
			3	-2555.16097	
Cr(II)	[CrPhCl ₃] ⁻	PBE0	1	-2656.39646	-33.31
			3	-2656.44955	
Cr(II)	CrPhCl ₂	PBE0	2	-2196.20995	-59.68 -75.69
			4	-2196.30506	
			6	-2196.33057	
Cr(III)	CrPhCl ₃	PBE0	2	-2656.35458	-24.42 13.18
			4	-2656.39349	
			6	-2656.33357	
Cr(V)	[CrPhCl ₃] ²⁺	PBE0	1	-2655.55977	5.73
			3	-2655.55064	
Mn(I)	[MnPhCl ₃] ²⁻	PBE0	1	-2762.81288	-23.55 -66.22
			3	-2762.85041	
			5	-2762.91841	
Mn(I)	MnPhCl	PBE0	1	-1842.67306	-6.50 -36.68
			3	-1842.68342	
			5	-1842.73151	
Mn(II)	MnPhCl ₂	PBE0	2	-2302.76584	-19.10 -53.92
			4	-2302.79628	
			6	-2302.85177	
Mn(IV)	[MnPhCl ₃] ⁺	PBE0	2	-2762.49734	-36.57 -23.24
			4	-2762.55561	
			6	-2762.53437	
Mn(V)	[MnPhCl ₃] ²⁺	PBE0	1	-2761.95828	-46.60 -47.48
			3	-2762.03255	
			5	-2762.03395	
Fe(II)	FePhCl ₂	PBE0	1	-2415.44017	-14.23 -38.76
			3	-2415.46285	
			5	-2415.50193	
Fe(III)	FePhCl ₃	PBE0	2	-2875.46512	-26.36
			4	-2875.50714	
Co(II)	CoPhCl ₂	PBE0	2	-2534.4861	-12.06 58.88
			4	-2534.50532	
			6	-2534.39226	

Table A-3 Energy difference between high- and low-spin magnetic states in transition metal ion-benzene (Ph) complexes (continued)

Metal Ion	Complex	DFT Functional	Spin State, $2S+1$	E (Hartree)	ΔE_{mag} (kcal/mol)
Ni(II)	NiPhCl ₂	PBE0	1	-2659.97365	
			3	-2659.99398	-12.76
			5	-2659.87838	59.78
Ni(III)	NiPhCl ₃	PBE0	2	-3119.99592	
			4	-3120.01725	-13.39
			6	-3119.88663	68.58

Table A-4 Energy difference between high- and low-spin magnetic states in transition metal ion-cycloheptatrienyl (Hp⁺) complexes

Metal Ion	Complex	DFT Functional	Spin State, 2S+1	E (Hartree)	ΔE_{mag} (kcal/mol)
V(II)	VHpCl ₃	PBE0	2	-2594.57251	36.61
			4	-2594.51416	
Cr(II)	CrHpCl ₃	PBE0	1	-2694.90808	-49.16 -51.95
			3	-2694.98643	
			5	-2694.99086	
Cr(III)	[CrHpCl ₃] ⁺	PBE0	2	-2694.65958	-56.11
			4	-2694.749	
			6		
Mn(II)	MnHpCl ₃	PBE0	2	-2801.40881	-49.15 -72.18
			4	-2801.48713	
			6	-2801.52384	
Fe(II)	FeHpCl ₃	PBE0	1	-2914.06604	-2.99 -68.32
			3	-2914.07081	
			5	-2914.17492	
Fe(III)	[FeHpCl ₃] ⁺	PBE0	2	-2913.77955	8.39
			4	-2913.76618	
Co(II)	CoHpCl ₃	PBE0	2	-3033.08797	-53.32 -8.99
			4	-3033.17295	
			6	-3033.10229	
Ni(II)	NiHpCl ₃	PBE0	1	-3158.62106	6.13 18.77
			3	-3158.61129	
			5	-3158.59114	
Ni(III)	[NiHpCl ₃] ⁺	PBE0	2	-3158.35824	60.16
			4		
			6	-3158.26236	

Table A-5 Energy difference between high- and low-spin magnetic states in transition metal ion-cyclooctatetraene ([COT]²⁻) complexes


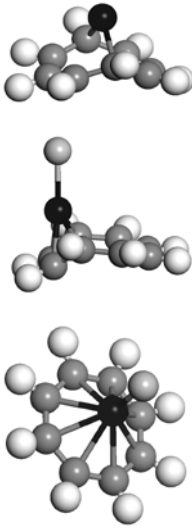
Metal Ion	Complex	Structure	DFT Functional	Spin State, 2S+1	E (Hartree)	ΔE_{mag} (kcal/mol)
V(II)	V(COT)	...	PBE0	1	-1252.90288	-29.10
				3	-1252.949255	
			B3LYP	1	-1253.493913	-24.14
				3	-1253.532379	
			HSE03	1	-1253.151167	-16.27
				3	-1253.1771	
Cr(III)	Cr(COT)Cl	...	PBE0	1	-1813.470457	-20.68
				3	-1813.503411	
Cr(II)	Cr(COT)		PBE0	2	-1353.340621	-27.96
				4	-1353.385175	
			B3LYP	2	-1353.939721	-23.41
				4	-1353.977031	
			HSE03	2	-1353.572457	-26.86
				4	-1353.615258	
Mn(II)	Mn(COT)		PBE0	1	-1459.766615	-72.07
				5	-1459.88146	
			B3LYP	1	-1460.412796	-42.84
				5	-1460.481068	
			HSE03	1	-1460.034791	-49.66
				5	-1460.113929	
Fe(III)	[Fe(COT)] ⁺ Fe(COT)Cl		HF	1	--	5.07
			PBE0	5	-1569.914411	
				1	-1572.296859	
			B3LYP	5	-1572.288777	
				1	-1572.920006	
			HSE03	5	-1572.922376	-1.49
				1	-1572.5329	
			PBE0	5	-1572.540011	-4.46
				1	-2032.616565	
			B3LYP	5	-2032.663545	-29.48
				1	-2033.429486	
			HSE03	5	-2033.446452	-10.65
				1	-2032.926909	
				5	-2032.948066	-13.28

Table A-5 Energy difference between high- and low-spin magnetic states in transition metal ion-cyclooctatetraene ([COT]²⁻) complexes (continued)


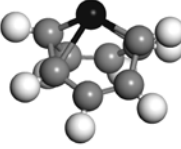
Metal Ion	Complex	Structure	DFT Functional	Spin State, 2S+1	E (Hartree)	ΔE_{mag} (kcal/mol)
Fe(II)	Fe(COT)		PBE0	0	-1572.458193	-51.70
			B3LYP	4	-1572.540577	
			HSE03	0	-1573.085564	-44.04
				4	-1573.155745	
				0	-1572.69417	-50.01
				4	-1572.773865	
Co(II)	Co(COT)	...	PBE0	1	-1691.480649	-43.06
			B3LYP	3	-1691.54927	
			HSE03	1	-1692.163048	-10.09
				3	-1692.179126	
				1	-1691.766314	-11.66
				3	-1691.784899	
Ni(III)	Ni(COT)Cl	...	PBE0	1	-2277.177861	3.90
				3	-2277.171639	
Ni(II)	Ni(COT)		PBE0	0	-1816.923405	75.40
			B3LYP	2	-1816.803252	
			HSE03	0	-1817.568768	-80.45
				2	-1817.696978	
				0	-1817.307678	11.44
				2	-1817.289441	

Table A-6 Energy difference between high- and low-spin magnetic states in transition metal ion-pyrrole (Py) complexes




Metal Ion	Complex	Structure	DFT Functional	Spin State, $2S+1$	E (Hartree)	ΔE_{mag} (kcal/mol)
Cr(II)	CrPyCl ₂		PBE0	2 4	-2174.256742 -2174.293651	-23.16
Mn(II)	MnPyCl ₂		PBE0	1 5	-2280.715037 -2280.82386	-68.29
Fe(II)	[FePy] ²⁺		HF	0 4	-1470.644221 -1470.740657	-60.51
			PBE0	0 4	-1472.500893 -1472.575717	-46.95
			B3LYP	0 4	-1472.997941 -1473.062156	-40.30
			HSE03	0 4	-1472.677264 -1472.741404	-40.25
	[FePyCl] ⁺		HF	0 4	-1930.652465 --	
			PBE0	0 4	-1933.056694 -1933.12817	-44.85
			B3LYP	0 4	-1933.724937 -1933.783817	-36.95
			HSE03	0 4	-1933.284878 -1933.35085	-41.40
	FePyCl ₂		PBE0	0 2 4	-2393.39154 -2393.421948 -2393.474424	-19.08 -52.01
			B3LYP	0 4	-2394.221505 -2394.297869	-47.92
			HSE03	0 4	-2393.66438 -2393.745053	-50.62

Table A-7 Energy difference between high- and low-spin magnetic states in transition metal ion-imidazole (Imid) complexes





Metal Ion	Complex	Structure	DFT Functional	Spin State, $2S+1$	E (Hartree)	ΔE_{mag} (kcal/mol)
Cr(II)	Cr(Imid)Cl ₂		PBE0	2 4	-2190.273369 -2190.356811	-52.36
Mn(II)	Mn(Imid)Cl ₂		PBE0	1 5	-2296.748122 -2296.879117	-82.20
Fe(II)	[Fe(Imid)] ²⁺		PBE0	0 4	-1488.491421 -1488.618035	-79.45
			B3LYP	0 4	-1489.000355 --	
			HSE03	0 4	-1488.670679 --	
	[Fe(Imid)Cl] ⁺		PBE0	0 4	-1949.06401 -1949.179728	-72.61
			B3LYP	0 4	-1949.741627 -1949.850607	
			HSE03	0 4	-1949.292257 -1949.40474	
	Fe(Imid)Cl ₂		PBE0	0 4	-2409.406799 -2409.502944	-60.33
			B3LYP	0 4	-2410.249549 -2410.338716	
			HSE03	0 4	-2409.682977 -2409.776905	
			PBE0	0 4	-2409.406799 -2409.502944	-60.33
			B3LYP	0 4	-2410.249549 -2410.338716	
			HSE03	0 4	-2409.682977 -2409.776905	

Table A-8 Energy difference between high- and low-spin magnetic states in transition metal ion-thiophene (Thio) complexes

Metal Ion	Complex	DFT Functional	Spin State, $2S+1$	E (Hartree)	ΔE_{mag} (kcal/mol)
Cr(II)	Cr(Thio)Cl ₂	PBE0	2	-2516.994806	-21.33
			4	-2517.028793	
Mn(II)	Mn(Thio)Cl ₂	PBE0	1	-2623.455421	-62.28
			5	-2623.554667	
Fe(II)	[Fe(Thio)] ²⁺	PBE0	0	-1815.226675	-47.51
			4	-1815.302382	
	[Fe(Thio)Cl] ⁺	PBE0	0	-2275.792916	-40.87
			4	-2275.858054	
	Fe(Thio)Cl ₂	PBE0	0	-2736.129101	-49.94
			4	-2736.208693	

INTENTIONALLY LEFT BLANK.

List of Symbols, Abbreviations, and Acronyms

C	carbon
Co	cobalt
COT	cyclo-octatetraene, $(C_8H_8)^{2-}$
Cp	cyclopentadienyl, $(C_5H_5)^-$
Cr	chromium
Cu	copper
DFT	density functional theory
Fe	iron
Hp	cycloheptatrienyl, $(C_7H_7)^+$
Imid	imidazole, $C_3N_2H_4$
Mn	manganese
N	nitrogen
Ni	nickel
PANI	polyaniline
Ph	benzene, C_6H_6
Py	pyrrole, C_4NH_5
S	sulfur
Sc	scandium
Thio	thiophene, C_4SH_4
Ti	titanium
V	vanadium

Nomenclature

Z	atomic number
S	spin state

ΔE_{mag}	magnetic stabilization energy
J	magnetic coupling constant
T	temperature
C_V	heat capacity
B	magnetic field
M	magnetization
χ	magnetic susceptibility
μ	magnetic permeability
μ_r	relative magnetic permeability
μ_0	permeability of free space, $4\pi \times 10^{-7} \text{ N/A}^2$
μ_B	Bohr magneton, $9.274 \times 10^{-24} \text{ J/T}$

1 DEFENSE TECHNICAL
(PDF) INFORMATION CTR
DTIC OCA

2 DIRECTOR
(PDF) US ARMY RESEARCH LAB
RDRL CIO LL
IMAL HRA MAIL & RECORDS MGMT

1 GOVT PRINTG OFC
(PDF) A MALHOTRA

17 DIR USARL
(PDF) RDRL SEE B
H DONG
RDRL SER M
S KELLER
A ZAGHLOUL
RDRL WML B
D TAYLOR
RDRL WMM
R DOWDING
J ZABINSKI
RDRL WMM C
J LA SCALA
RDRL WMM D
R BRENNAN
S WALSH
RDRL WMM E
J LASALVIA
RDRL WMM G
J ANDZELM
F BEYER
J LENHART
R MROZEK
A RAWLETT
B RINDERSPACHER
J SNYDER

INTENTIONALLY LEFT BLANK.